SUPERSYMMETRY OR STELLAR PHYSICS : COSMIC RAY ELECTRONS AND POSITRON EXCESSES

Peter L. Biermann[1,2,3,4,5], Julia K. Becker[6,7], Athina Meli[8], Wolfgang Rhode[7], Eun-Suk Seo[9], & Todor Stanev[10]

[1] MPI for Radioastronomy, Bonn, Germany
[2] Dept. of Phys. & Astron., Univ. of Bonn, Germany
[3] Dept. of Phys. & Astr., Univ. of Alabama, Tuscaloosa, AL, USA
[4] Dept. of Phys., Univ. of Alabama at Huntsville, AL, USA
[5] FZ Karlsruhe, and Phys. Dept., Univ. Karlsruhe, Germany

[6] Institution för Fysik, Göteborgs Univ., Sweden
[7] Dept. of Phys., Univ. Dortmund, Dortmund, Germany
[8] ECAP, Friedrich-Alexander Universität Erlangen-Nürnberg, Germany
[9] Dept. of Physics, Univ. of Maryland, College Park, MD, USA
[10] Bartol Research Inst., Univ. of Delaware, Newark, DE, USA

www.mpifr-bonn.mpg.de/div/theory

Cosmic ray electrons and positrons: new data

- Pamela: 0810.4995: positron fraction increasing with energy
- ATIC: Nature **456**, 362 (2008): "flat" feature in cosmic ray electrons
- H.E.S.S.: 0811.3894: "steep" feature in cosmic ray electrons

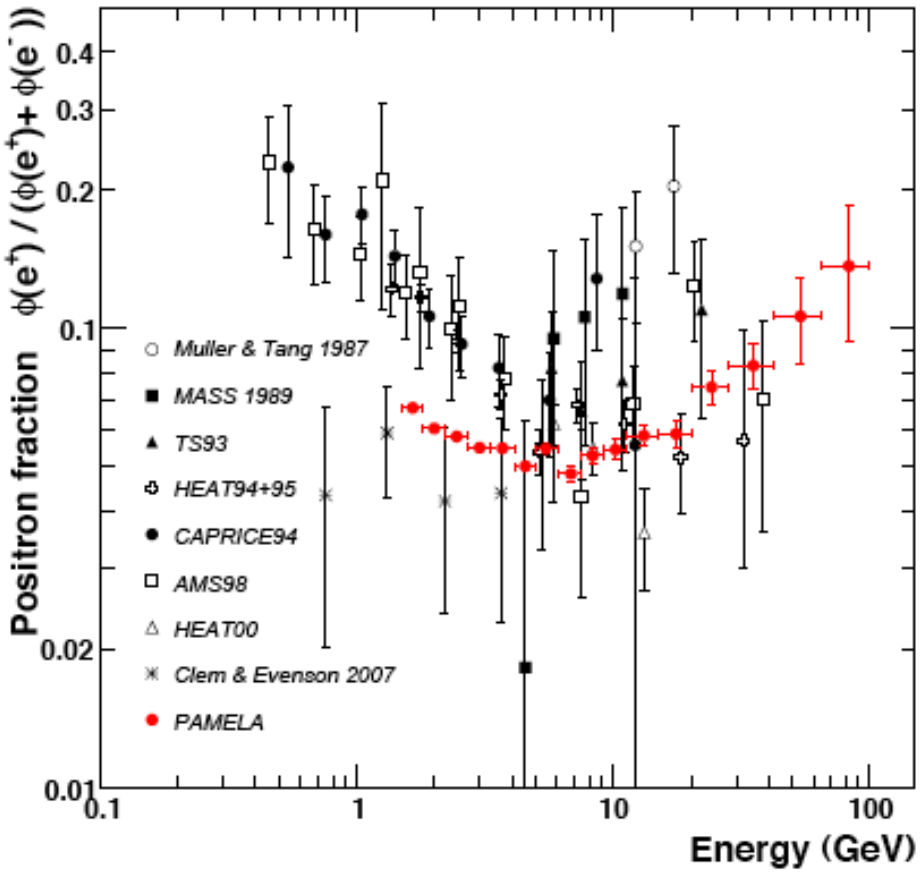

FIG. 3: **PAMELA positron fraction with other experimental data.** The positron fraction measured by the PAMELA experiment compared with other recent experimental data[24, 29, 30, 31, 32, 33, 34, 35]. One standard deviation error bars are shown. If not visible, they lie inside the data points.

Figure 1 Pamela data on positron fraction, 2008

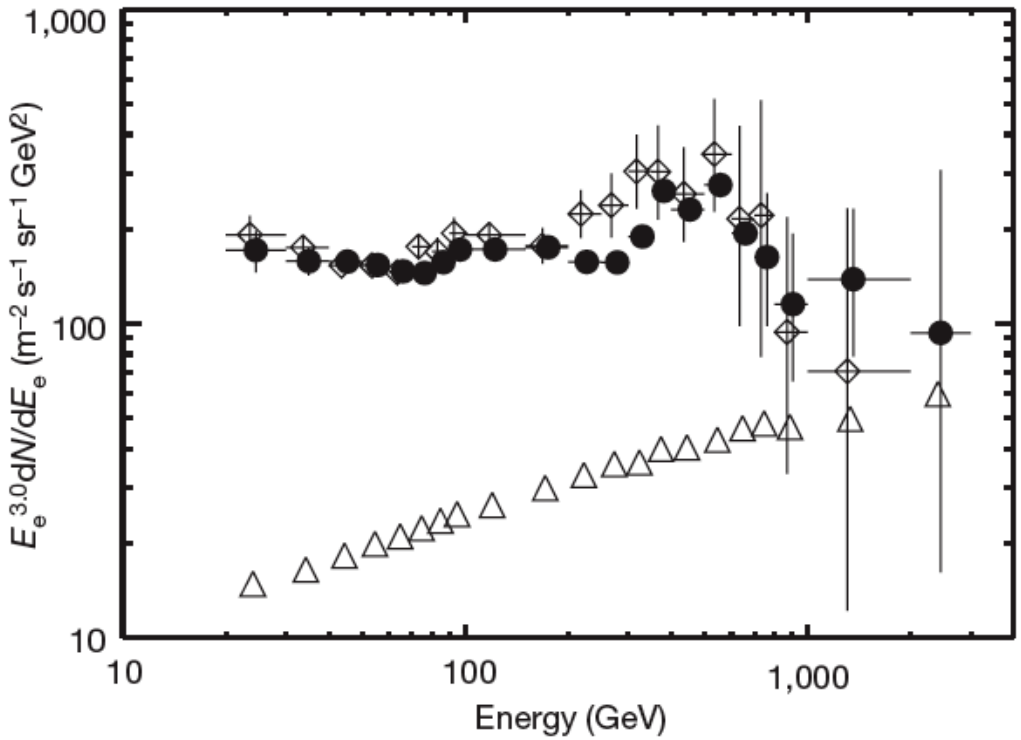

Figure 2 | ATIC-1 and ATIC-2 spectra at balloon altitude, showing good agreement with each other. The measured primary electron flux (scaled by E^3) at flight altitude is shown for ATIC-1 (open squares) and ATIC-2 (filled circles). The errors are one standard deviation. Both balloon flights were from McMurdo, Antarctica, and circumnavigated that continent. ATIC-1 was a test flight in 2000–01 and the usable data correspond to an exposure of 0.61 m^2 sr days. ATIC-2 was a science flight in 2002–03 with an exposure of 2.47 m^2 sr days. To eliminate edge effects, we restrict the incident zenith angle to be less than $\sim 37^\circ$ ($\cos\theta \geq 0.8$), use only the central 80% of the SiM

Figure 2 ATIC data on cosmic ray electrons, 2008; open triangles background

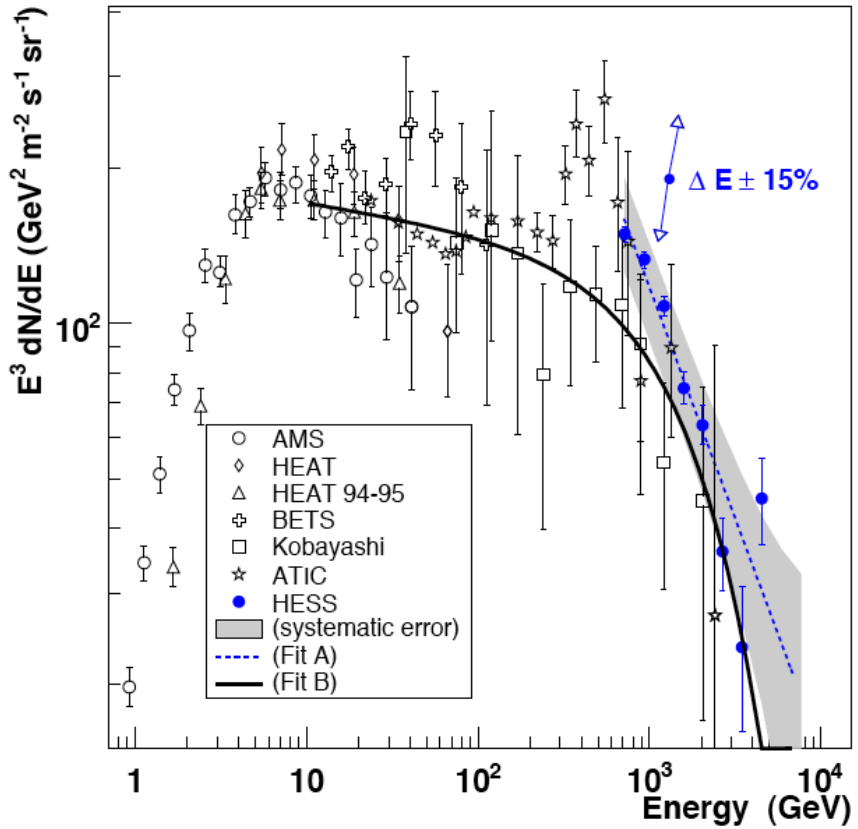

FIG. 3: The energy spectrum E^3 dN/dE of CR electrons as measured by H.E.S.S. in comparison with previous measurements. The H.E.S.S. data are shown as solid points. The two fit functions (A and B) are described in the main text. Upper limits are given for a confidence level of 95%. The shaded band indicates the approximate systematic error arising from uncertainties in the modeling of hadronic interactions and in the atmospheric model. The double arrow indicates the ef-

Figure 3 H.E.S.S. data on cosmic ray electrons, 2008

Some suggestions

- L. Bergström et al., 0808.3725: Positrons from SUSY dark matter
- V. Barger et al., 0809.0162: Dark matter lighter than the top quark
- J.H. Huh et al, 0809.2601, 2008: Two DM components and MSSM
- Yüksel et al., 0810.2784: TeV gamma rays from Geminga...

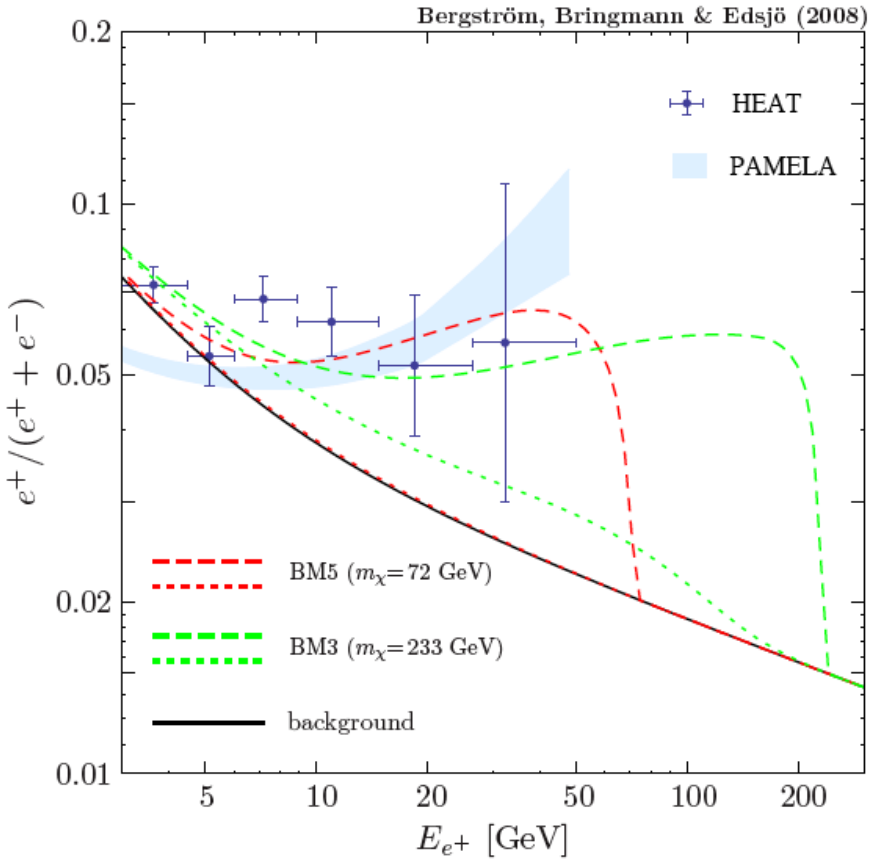

FIG. 3: The solid line is the expected flux ratio $e^+/(e^+ + e^-)$ as calculated following [32]. The data points are the combined HEAT data [33] and the light shaded area roughly corresponds to the (so far unpublished) PAMELA data [5]. Furthermore, the expected flux ratio for our benchmark models is shown without (dotted lines) and after taking into account radiative corrections (dashed lines). See text for further details.

Figure 4 L. Bergström et al., 0808.3725, 2008: Neutralino annihilation

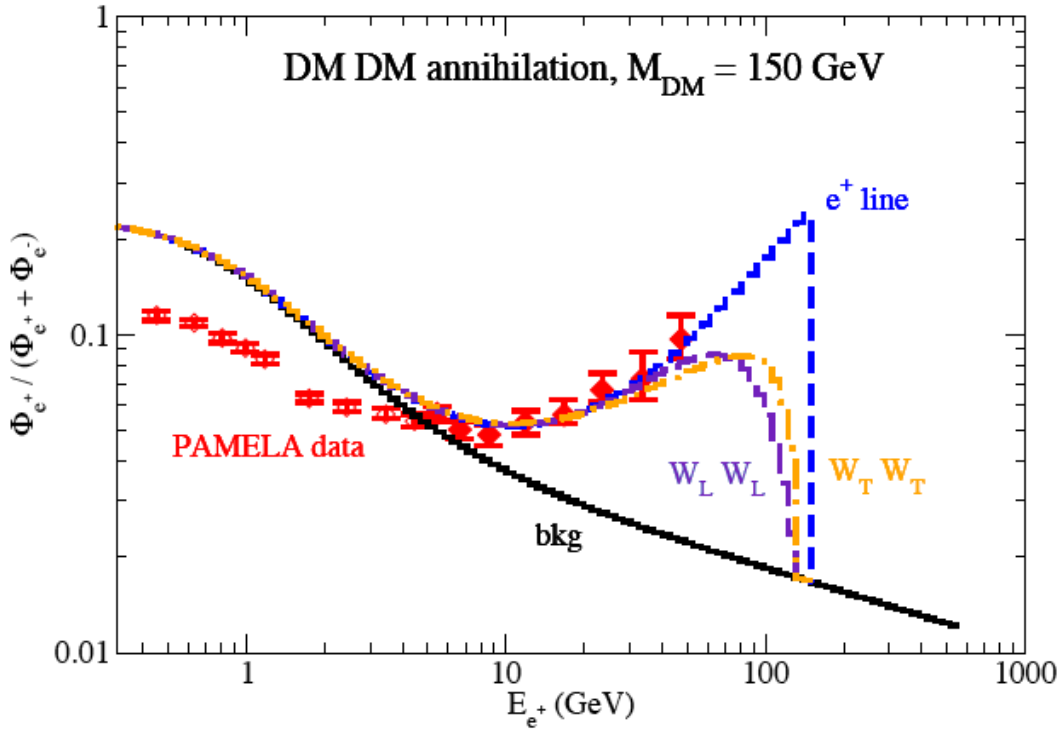

FIG. 1: Annhilations of DM directly into e^+e^- give the e^+ line at about $M_{DM} = 150$ GeV. The secondary positron spectrum from decays of longitudinal (transverse) W bosons is labeled W_LW_L (W_TW_T). The data points are preliminary results from the PAMELA experiment. Only data points above 5 GeV (denoted by filled symbols) are included in our analysis. The solid curve is the expected background. The med set of propagation parameters is used with the NFW profile for the DM halo.

Figure 5 V. Barger et al., 0809.0162, 2008: DM annihilation lighter than top quark

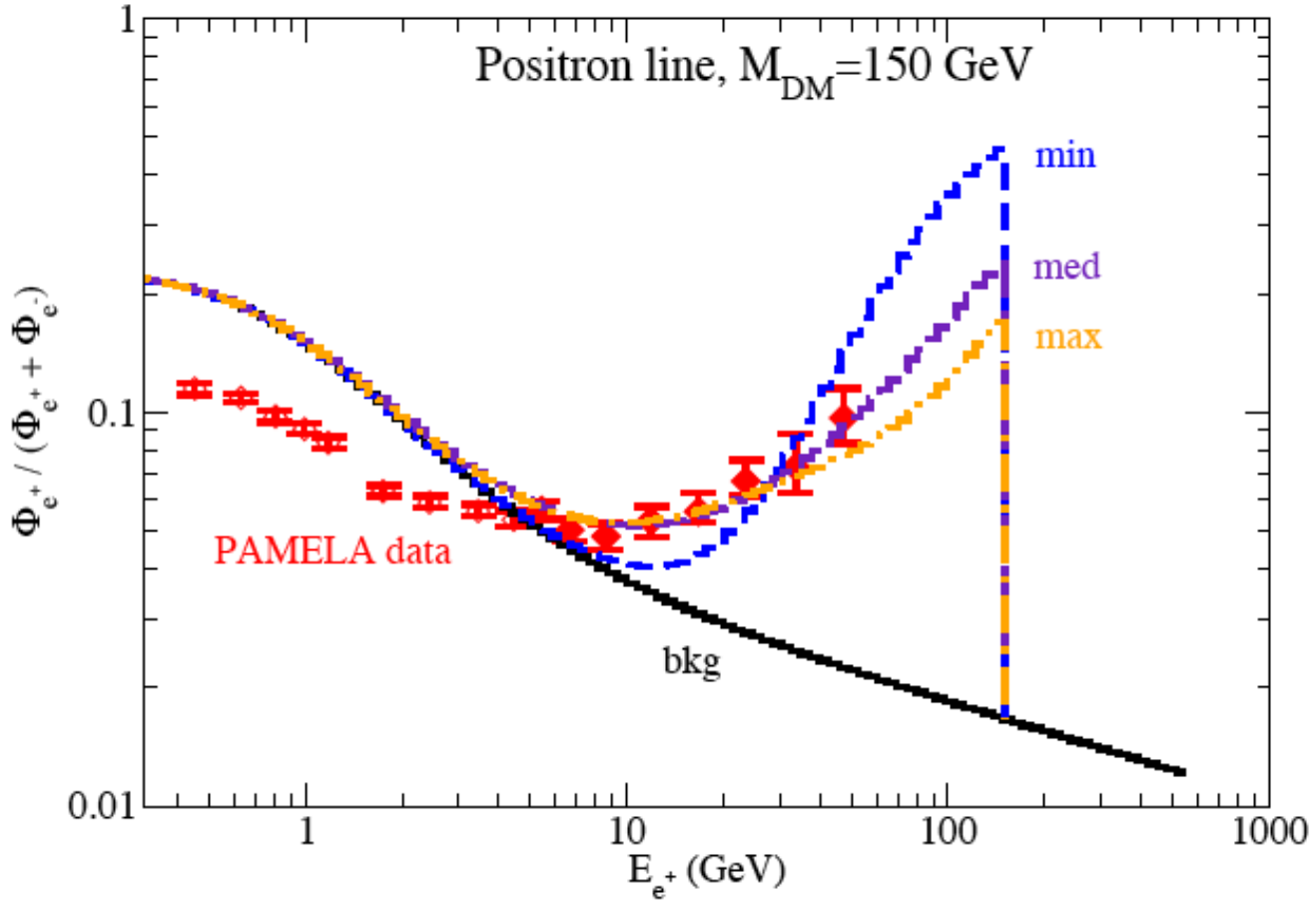

FIG. 3: The effect of propagation on the e^+ line spectrum is depicted by considering the min, med and max sets for DM that is assumed not to annihilate into W pairs. The min set does not yield a spectrum consistent with the data.

Figure 6 V. Barger et al., 0809.0162, 2008: DM annihilation lighter than top quark

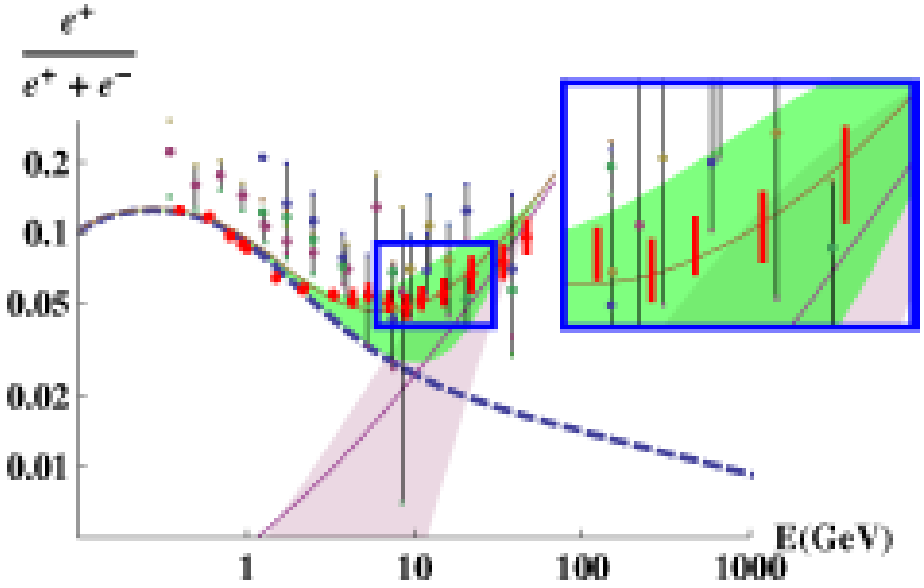

FIG. 4: *The posttron fraction from our model with* $M_\chi = 200$ *GeV,* $m_N = 80$ *GeV,* $m_E = 200$ *GeV and* $M_z = 220$ *GeV and* $B = 9$. *The pink band is the posttron fraction coming from* χN *annhilation and the green band is this posttron excess on top of the astrophysical background (the thick blue dash line is from the astrophysical background [18, 19]). The red points are the preliminary PAMELA data [17]. The width of the band shows the uncertainty from the posttron propagation model. The various small spots represents the observed posttron cosmic ray data [21, 22, 23, 24].*

Figure 7 J.H. Huh et al, 0809.2601, 2008: annihilation between two different components of DM

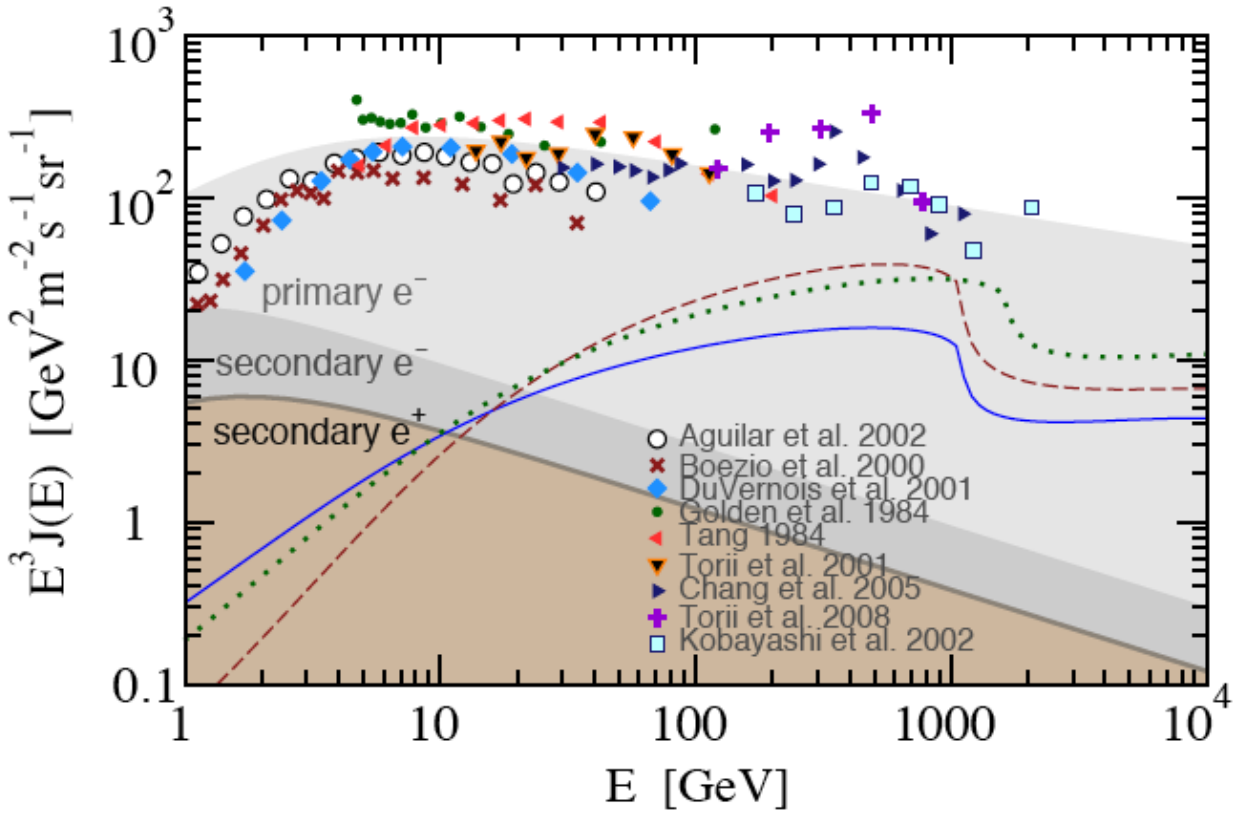

FIG. 3: Cosmic-ray electron and positron spectra. Shown are models from Ref. [10] (shades), electron data compiled in Ref. [25], and additional contributions to the positron flux from our Geminga scenarios (solid, dashed, and dotted lines) to be compared to secondary positrons (lowest shade).

Figure 8 Yüksel et al., 0810.2784, 2008: Geminga TeV pulsar wind nebula

Massive stars

- Stars between 8 and 15 $M_\odot$ explode into the ISM
- Stars above 15 $M_\odot$ explode into their own stellar wind
- Stellar winds have $B_r \sim r^{-2}$, and $B_\phi \sim (\sin\theta)/r$ (Parker 1958)
- Explosions into the ISM give $E^{-2.42}$, the predicted injection limit
- Diffusive losses add factor $E^{-1/3}$, so a spectrum of $E^{-2.75}$, the diffusion limit
- Theory error bars typically ± 0.04 in the spectrum

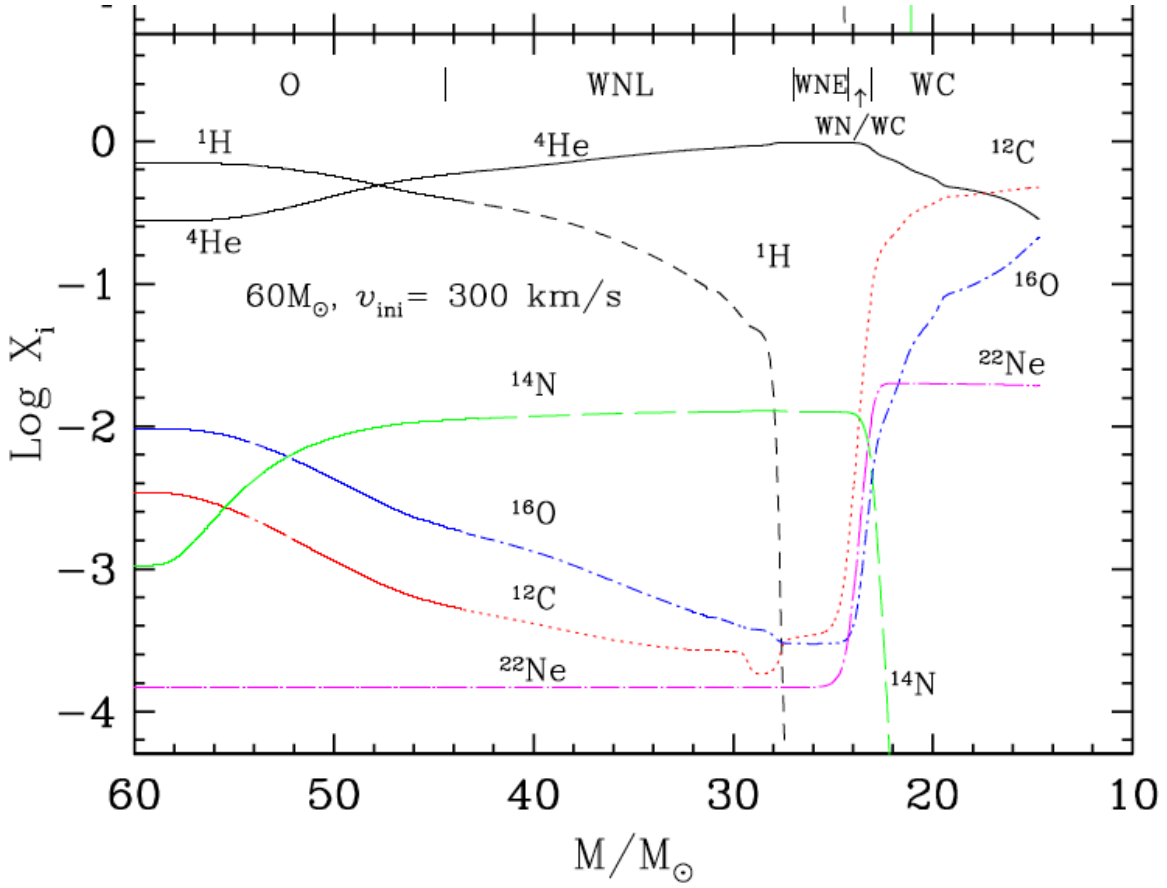

Figure 5. Evolution as a function of the actual mass of the abundances (in mass fraction) at the surface of a non–rotating (upper panel) and a rotating (lower panel) 60 $M_{\odot}$stellar model of solar composition (Meynet & Maeder 2003).

Figure 9 Maeder & Meynet ASP 388, 3, 2006, here lower panel of Fig. 5

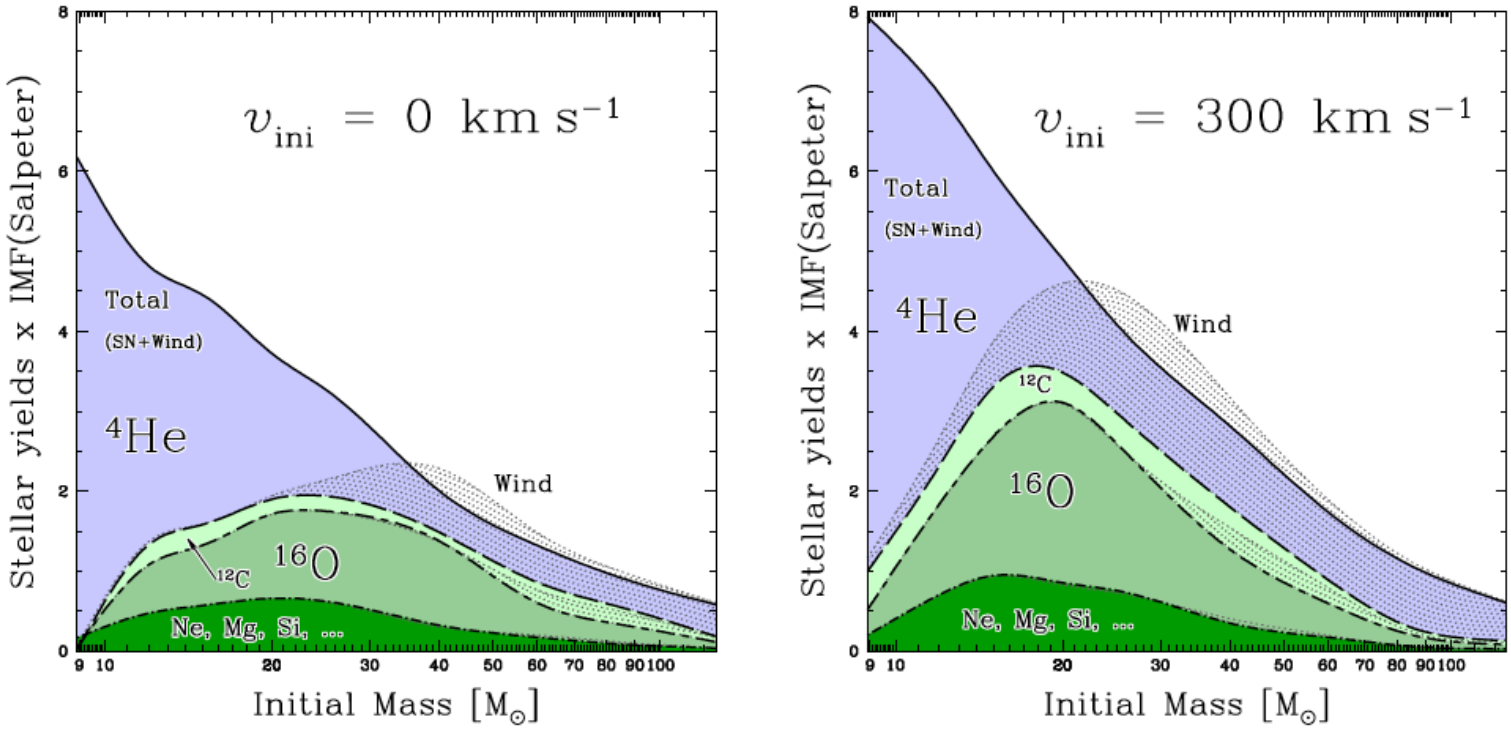

Figure 9. Product of the stellar yields, $mp_{im}^{\rm tot}$ by Salpeter's IMF (multiplied by an arbitrary constant: 1000 x $M^{-2.35}$), as a function of the initial mass for non–rotating (left) and rotating (right) models at solar metallicity. The different shaded areas correspond from top to bottom to $mp_{im}^{\rm tot}$ x 1000 x $M^{-2.35}$ for ^{4}He, ^{12}C, ^{16}O and the rest of the heavy elements. The dotted areas show for ^{4}He, ^{12}C and ^{16}O the wind contribution. Note that for ^{4}He, the total yields is smaller than the wind yields due to negative SN yields (Hirschi et al. 2004).

Figure 10 Maeder & Meynet ASP 388, 3, 2006, Fig. 9

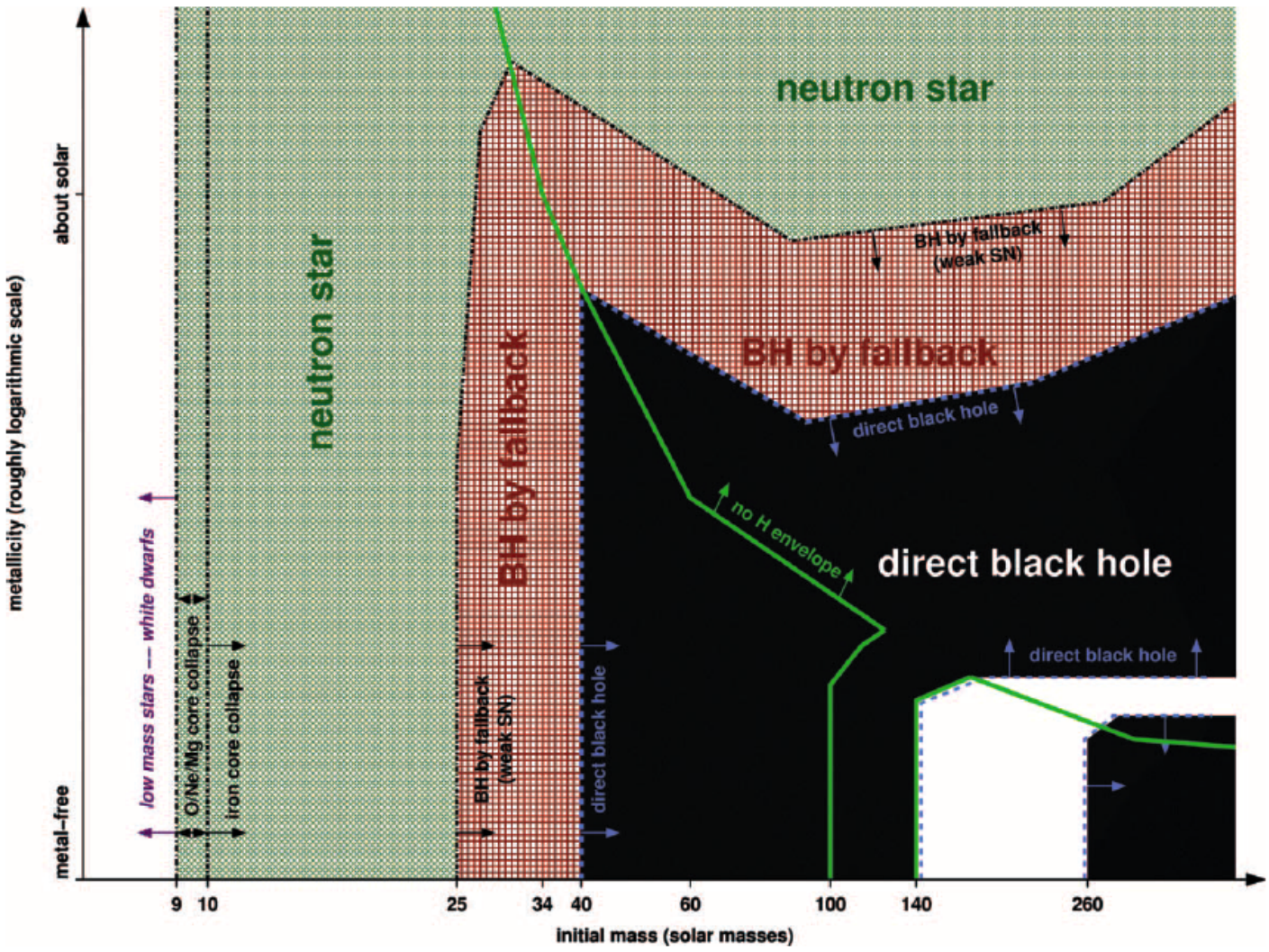

FIG. 1.—Remnants of massive single stars as a function of initial metallicity (*y-axis*; qualitatively) and initial mass (*x-axis*). The thick green line separates the regimes where the stars keep their hydrogen envelope (left and lower right) from those where the hydrogen envelope is lost (upper right and small strip at the bottom between 100 and 140 $M_{\odot}$). The dashed blue line indicates the border of the regime of direct black hole formation (*black*). This domain is interrupted by a strip of pair-instability supernovae that leave no remnant (*white*). Outside the direct black hole regime, at lower mass and higher metallicity, follows the regime of BH formation by fallback (*red cross-hatching and bordered by a black dot-dashed line*). Outside of this, green cross-hatching indicates the formation of neutron stars. The lowest mass neutron stars may be made by O/Ne/Mg core collapse instead of iron core collapse (*vertical dot-dashed lines at the left*). At even lower mass, the cores do not collapse and only white dwarfs are made (*white strip at the very left*).

Figure 11 Heger et al. ApJ 591, 288 (2003), Fig. 1

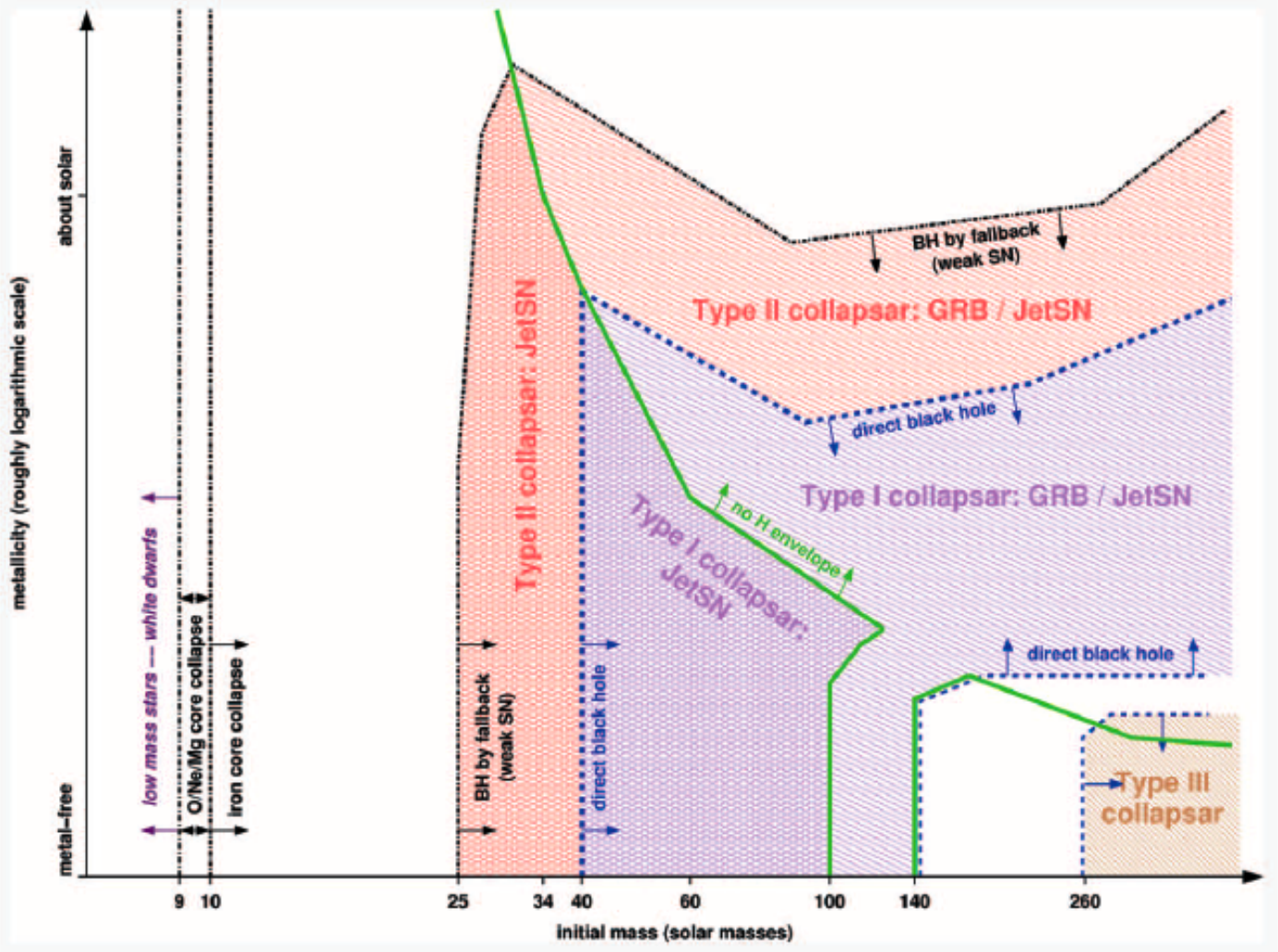

FIG. 3.—Collapsar types resulting from single massive stars as a function of initial metallicity and initial mass. Lines have the same meaning as in Fig. 1. Our main distinction is between collapsars that form from fallback (Type II; *red*) and directly (Type I; *pink*). We subdivide these into those that have a hydrogen envelope (*cross-hatching*), only able to form jet-powered supernovae (JetSNe) and hydrogen-free collapsars (*diagonal cross-hatching*), possibly making either JetSNe or GRBs (see also Fig. 4). The first subclass is located below the thick green line of loss of the hydrogen envelope, and the second is above it. The light brown diagonal hatching at high mass and low metallicity indicates the regime of very massive black holes formed directly (Type III collapsars) that collapse on the pair-instability and photodisintegration. Since the collapsars scenario require the formation of a BH, at low mass (left in the figure) or high metallicity (top of the figure) and in the strip of pair-instability supernovae (lower right) no collapsars occur (*white*).

Figure 12 Heger et al. ApJ 591, 288 (2003), Fig. 3

TABLE 4

REMNANT AND SUPERNOVA POPULATION YIELDS FOR DIFFERENT METALLICITIES, IMFS, AND MASS LIMITS

	Zero Metallicity				Solar Metallicity	
	High $M_{\rm FBH}^{\rm lim}$		Low $M_{\rm FBH}^{\rm lim}$		High $M_{\rm FBH}^{\rm lim}$	Low $M_{\rm FBH}^{\rm lim}$
Object	$\rm IMF_{Sal}$	$\rm IMF_{NU}$	$\rm IMF_{Sal}$	$\rm IMF_{NU}$	$\rm IMF_{Sal}$	$\rm IMF_{Sal}$
Remnants						
NS	75	56	66	50	87	75
BH	23	36	32	43	13	25
MBH	0.9	3.0	0.9	3.0	0	0
Supernovae						
IIp strong	75	56	66	50	77	70
IIp weak	12	8.9	21	16	0	6.9
IIL/b	0	0	0	0	6.4	6.4
Ib/c strong	0	0	0	0	9.2	5.1
Ib/c weak	0	0	0	0	7.6	12
Other Outbursts						
Pulsar pair	1.4	4.7	1.4	4.7	0	0
Pair SNe	1.4	4.6	1.4	4.6	0	0
Jet SNe	24	39	33	46	13	25
GRBs	1.4	3.4	1.4	4.7	7.8	12

NOTE.—For solar metallicity, we use the IMF by Salpeter 1955 ($\rm IMF_{Sal}$); for zero metallicity, we additionally supply the results for the IMF by Nakamura & Umemura 2001 ($\rm IMF_{NU}$). We give the results for two different lower mass limits for fall-back black hole formation ($M_{\rm FBH}^{\rm lim}$): *high* corresponds to 25 $M_\odot$ and *low* to 20 $M_\odot$ (Fryer 1999).

Figure 13 Heger et al. ApJ 591, 288 (2003), Tab. 4

Red Supergiant and Wolf Rayet star environments

- Stars above about 15 $M_\odot$ explode as red super-giant stars, short RSG stars
- Stars above about 25 $M_\odot$ explode as blue super-giant stars, or Wolf Rayet stars, short WR stars
- Explosions into the wind give predicted $E^{-7/3}$, with diffusion limit $E^{-8/3}$
- Theory error bars typically -0.02 ± 0.02 in the spectrum, asymmetric error distribution

The polar cap component

- Polar cap component $E^{-2.00}$, right up to knee (about $Z\,10^{15}$ eV)
- at injection energies only a few percent of total CR power
- Electrons beyond about 20 GeV in loss limit (Kardashev 1962): so spectrum $E^{-3.00}$
- Electrons injected from about 30 MeV (Protheroe & Biermann 1996)
- Therefore cosmic ray electron polar cap component appears earlier in particle energy by the ratio of the mass, say, of Fe, and the 30 MeV, so about a factor of 4000 to the left, in the hundreds of GeV

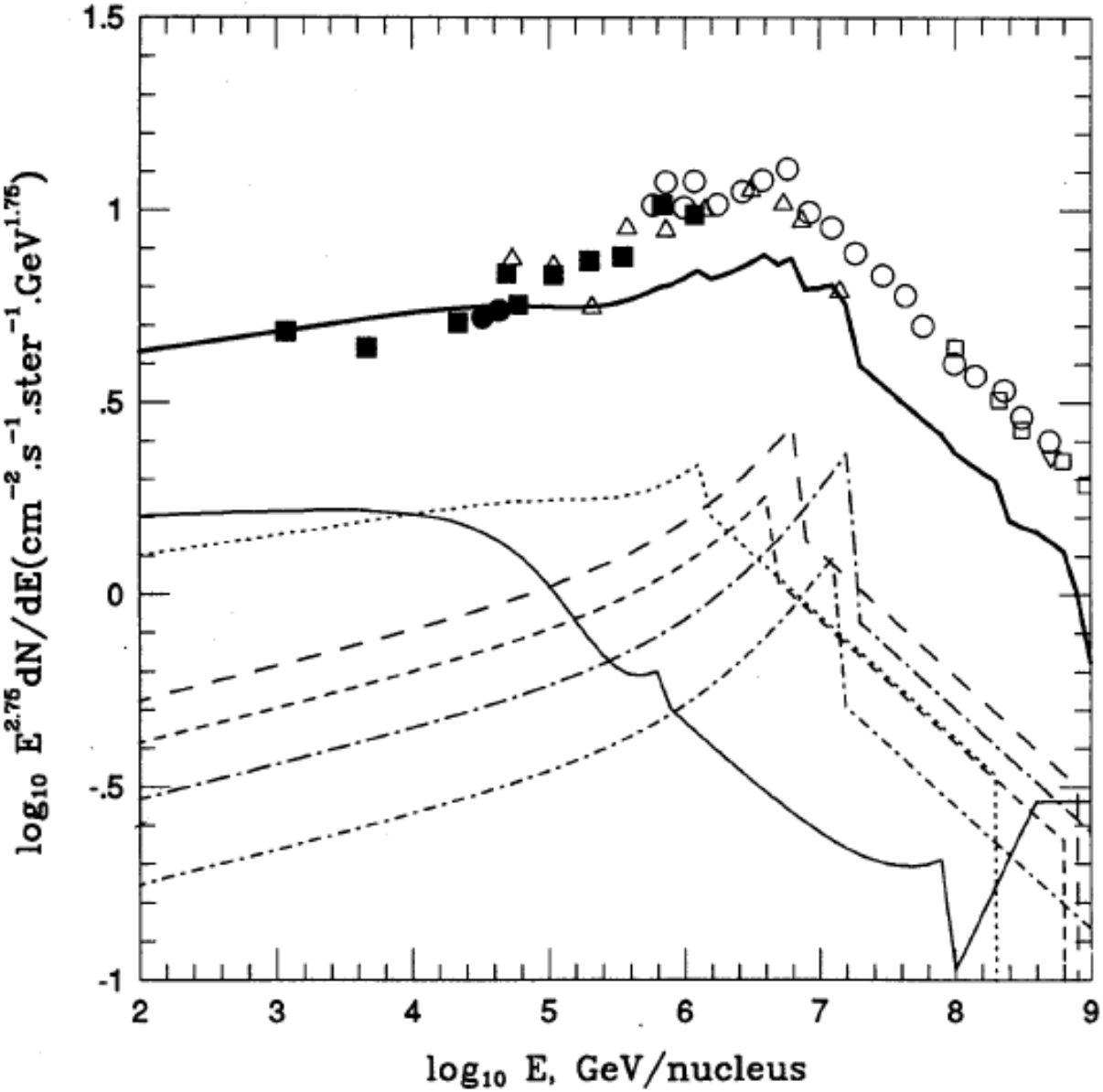

Figure 14 Spectral and chemical structure at the knee, to be repeated at high energy? Element groups are H, He, CNO, Ne-S, Cl-Mn, and Fe. Here the spectra are in the diffusion limit, and we need the injection limit; this implies multiplying all curves by $(A/Z)^{1/3} \simeq 10^{0.1}$. Source: Stanev et al., paper CR-IV 1993

Injection I

- We consider the excitation in a shocked region
- Cascade equation:

$$\frac{d}{dt}\frac{I(k)}{4\pi k^2} - \frac{1}{k^2}\frac{\partial}{\partial k}\left(\frac{k^4}{3\tau_k}\frac{\partial}{\partial k}\left(\frac{I(k)}{4\pi k^2}\right)\right) = A\delta(k-k_0)$$

- τ_k is the time scale of diffusion of turbulent energy:

$$\tau_k = \frac{1}{k(\gamma_{eff} I(k) k/\rho)^{1/2}}$$

- ρ matter density, γ_{eff} eff. adiab. index. Source k_0. Solution Kolmogorov (1941) cascade:
- $I(k) \sim k^2$ for $k \leq k_0$, and $I(k) \sim k^{-5/3}$ for $k \geq k_0$

Injection II

- Source term in cascade equation:
  $\sigma_{excit} \frac{I(k)}{4\pi k^2}$
  with
  $\sigma_{excit} = \frac{4\pi}{3} \frac{v_A}{I(k)k} p^4 v \frac{\partial f}{\partial x}$
- v particle velocity, f particle distribution function in p phase space, x local coordinate
- Distribution function has a step at a shock!
- Balance cascading with excitation, using a spectrum of the phase space distribution function (e.g. wind shock) of $p^{-7/3-2}$

Injection III

- Turbulence is excited by a) cosmic rays, and b) irregularities due to the instabilities in the wind-driving
- CR excited turbulence spectrum, $I(k) \sim k^{-13/9}$
- Irregularities inherent in wind-driving, $I(k) \sim k^{-2}$
- Concept: in WR stars the CR driving dominates, and in RSG stars the instability driving dominates
- Diffusion coefficient then $p^{5/9}$
- Secondary spallation products run as $E^{-5/9}$ steeper

$$\frac{N_{sec}}{N_{prim}} \sim E^{-5/9}$$

- This is consistent with the low energy Pamela data

Injection IV

- For RSG star explosions turbulence dominated by irregular motion, so
- $I(k) \sim k^{-2}$: secondary spallation no energy dependence

$$\frac{N_{sec}}{N_{prim}} \sim 1$$

-
- Test: γ-ray spectrum of the inner Galaxy, same as injection $E^{-7/3}$
- Modified by Solar wind modulation
- This is consistent with Milagro data for inner Galaxy

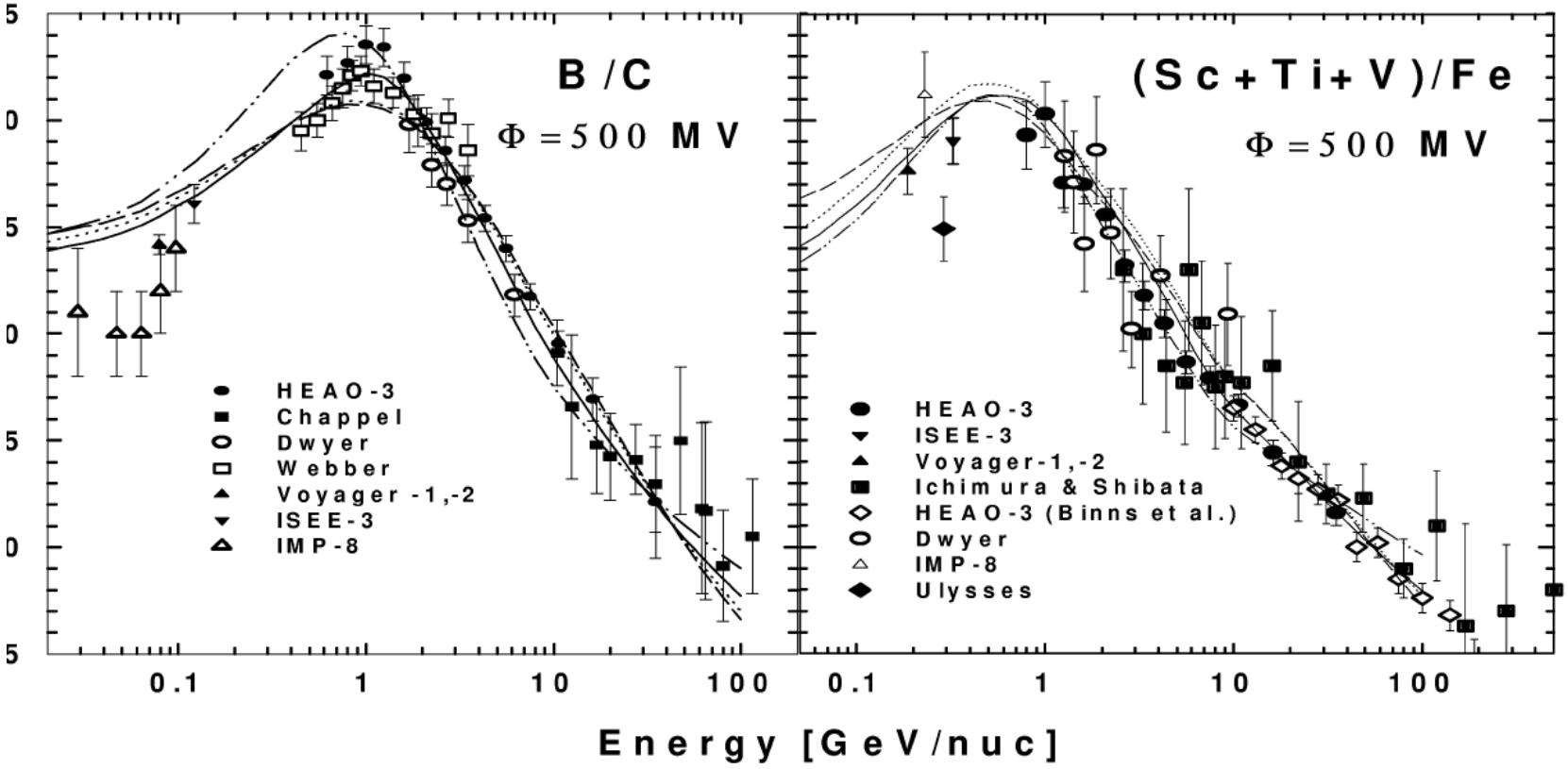

ure 1: The least squares fit to observed B/C and Sub-Fe/Fe ratios in four propagation models: turbulent usion (dashed lines), wind (dotted lines), reacceleration (dash-dotted lines), and the standard diffusion lel with the diffusion coefficient given by Eq. (2) (solid lines). Data are from a comprehensive npilation by Stephens & Streitmatter (1998).

Figure 15 Ptuskin et al., ICRC 1999, vol. 4, p. 291, Fig. 1: column $11.3\,\beta\,\mathrm{g/cm^2}$ for $R < 5\,\mathrm{GV}$ and $11.3\,\beta\,(R/5\,\mathrm{GV})^{-0.54}\,\mathrm{g/cm^2}$ for $R > 5\,\mathrm{GV}$; R is rigidity, i.e. momentum $\times c$/charge

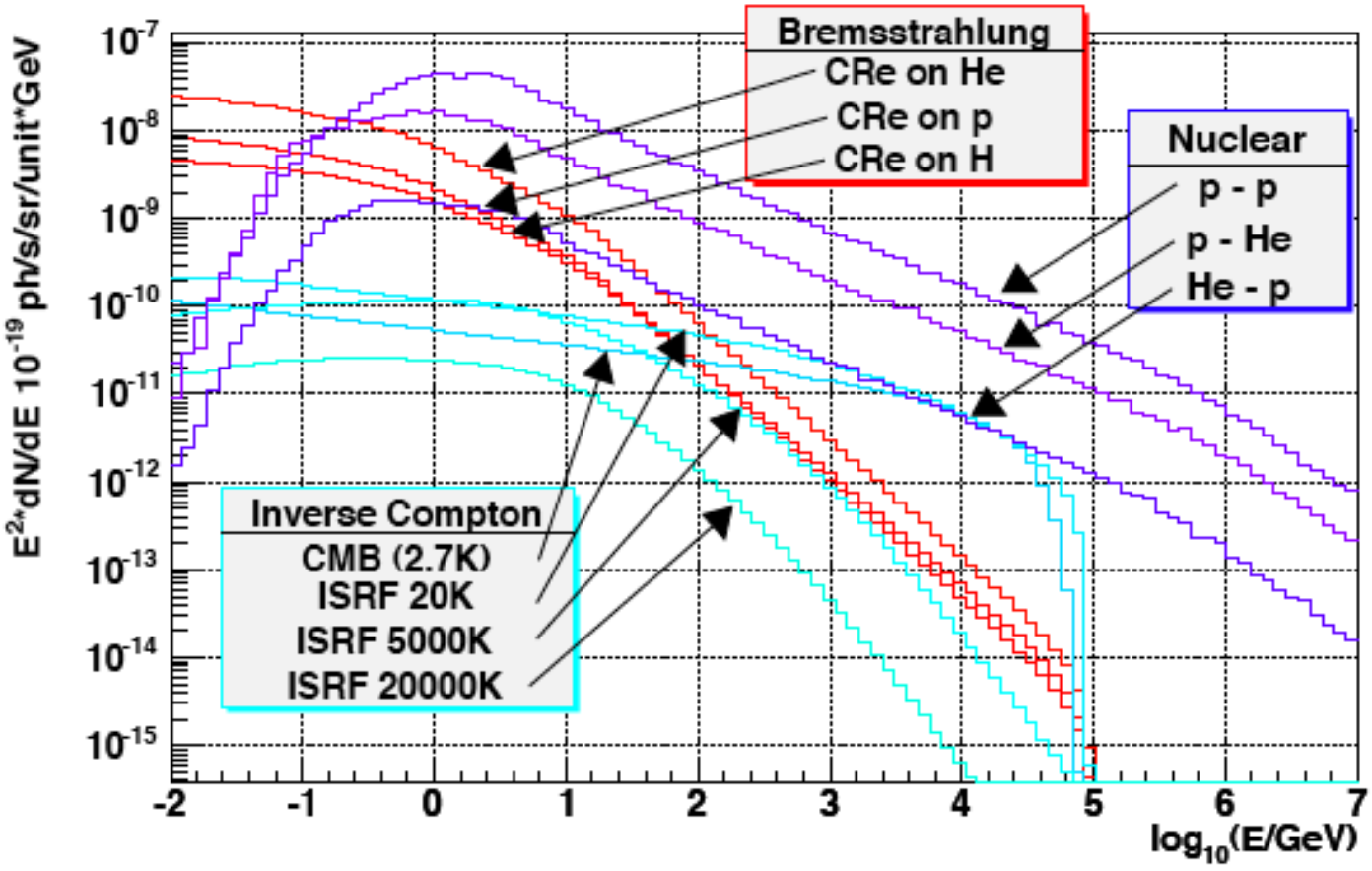

Figure 3. Gamma-ray production spectra, see Eq. (1). The spectra are shown in units of photons per atom, or cm^3 in the case of inverse Compton.

Figure 16 Casanova et al., Integral Meeting, 0403661, 2004, Fig. 3

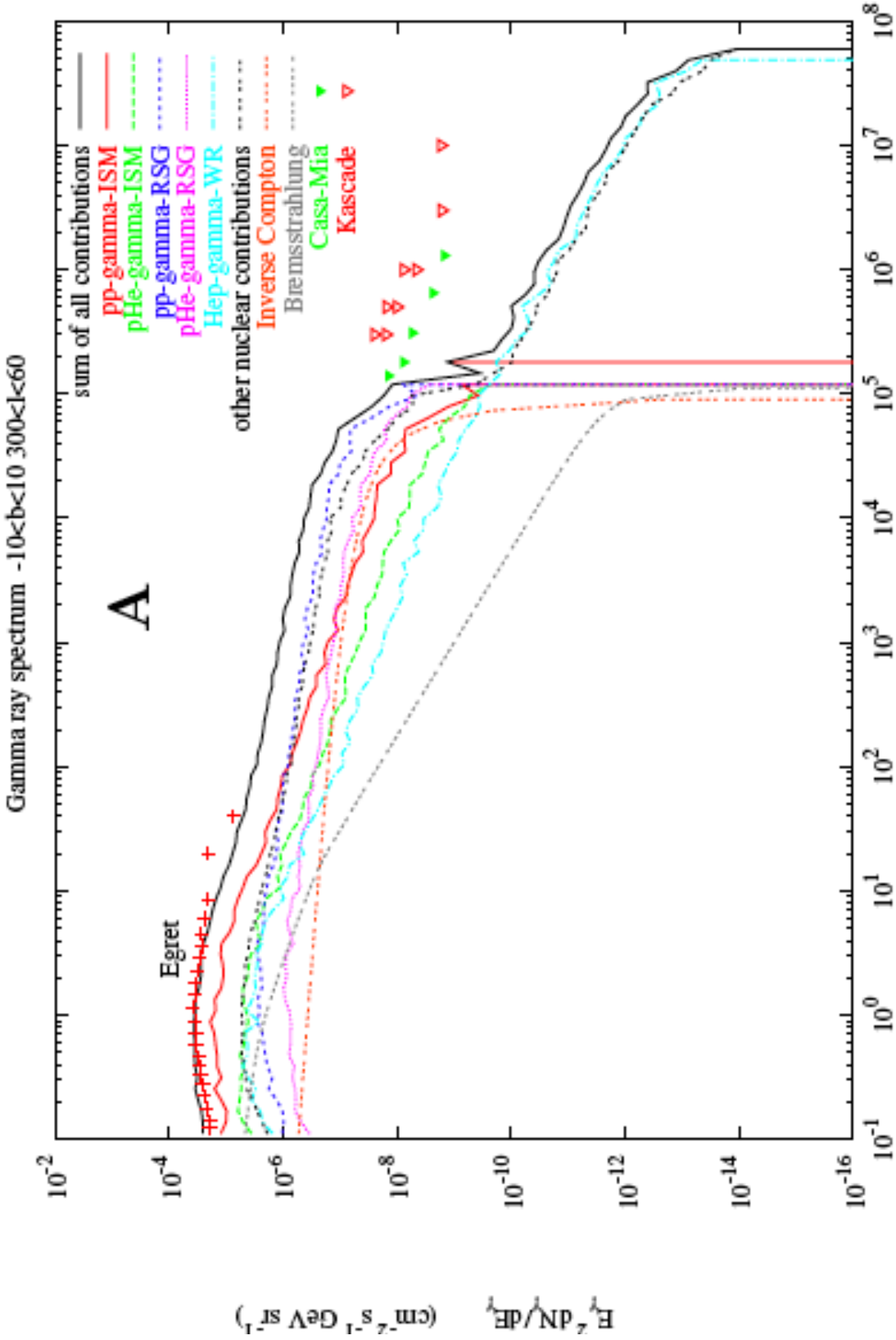

Figure 17 Casanova et al., Integral Meeting, 0403661, 2004, Fig. 5a, the inner Galaxy

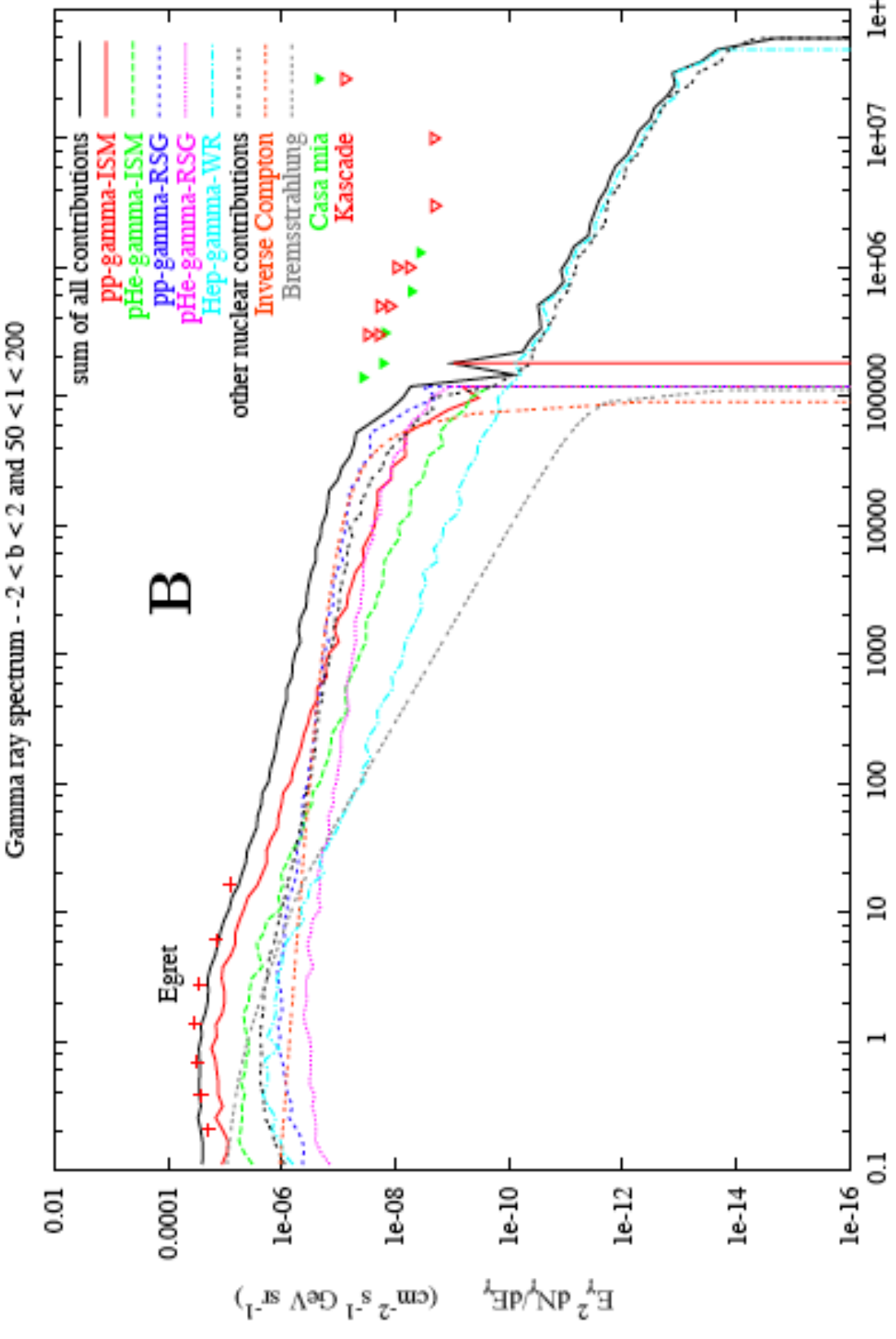

Figure 18 Casanova et al., Integral Meeting, 0403661, 2004, Fig. 5b, the outer Galaxy

Cosmic ray electrons and positrons

- Biermann, P.L., *Astron. & Astroph.* **271**, 649 (1993)
- Biermann, P.L., & **Cassinelli, J.P.**, *Astron. & Astroph.* **277**, 691 (1993)
- Stanev, T., Biermann, P.L:, & Gaisser, T.K., *Astron. & Astroph.* **274**, 902 (1993)
- Biermann, P. L., Gaisser, T. K., & Stanev, T., *Phys. Rev.* **D 51**, 3450 - 3454 (1995)
- Biermann, P.L., inv. lecture at the Nuclear Astrophysics meeting at Hirschegg, in Proc., GSI, Darmstadt, p. 211 - 222 (1998)
- Biermann, P.L., **Langer, N.**, Seo, E.-S., & Stanev, T., *Astron. & Astroph.* **369**, 269 - 277 (2001)

Injection V

- Injection of secondaries depends on production rate
- Acceleration faster for perpendicular shocks, so over most of $4\,\pi$, so reduced production of secondaries relative polar cap
- By $c/(3V_{sh})$, so a factor less than 10, probably more like 2 - 3 effectively (see Meli & Biermann 2006)
- This translates into a particle energy, where the polar cap component becomes dominant, conservatively between 2^3 to 3^3 lower than for electrons.
- This implies then an energy of 500 GeV divided by this factor, so 60 to 16 GeV. 30 GeV compatible with data.
- Therefore the ratio of the positron to electron fluxes should scale as $E^{+1/3}$
- This is consistent with the higher energy Pamela data.

Injection VI

- Integrating past injection at synchrotron loss limit gives $N(E) \sim E^{-7/3-1}$
- Random walk from nearby regions with $r \simeq \Delta r \sqrt{N}$
- Corresponding to a time $t \simeq \frac{\Delta r}{c} N$
- $$r \simeq \Delta r \sqrt{\frac{t\,c}{\Delta r}} \simeq \sqrt{t\,c\,\Delta r} \qquad (1)$$
- $\Delta r \sim E^{1/3}$, and $t \sim 1/E$, so $r \sim E^{-2/3}$
- Flat disk source distribution $\pi r^2 \simeq E^{-4/3}$
- So CR-e high energy spectrum predicted to be $\simeq E^{-3-4/3}$
- This is consistent with the H.E.S.S. data

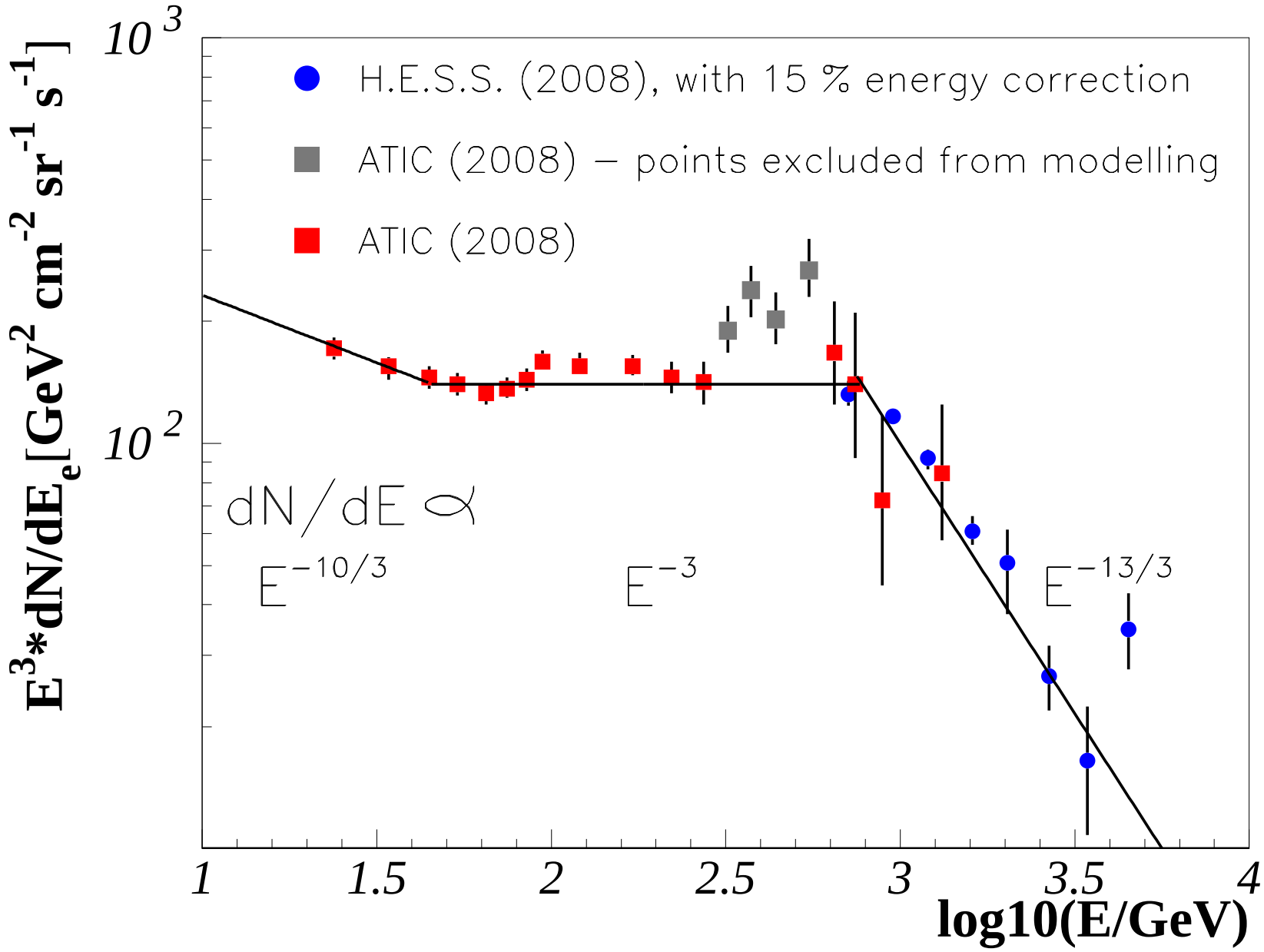

Figure 19 Model prediction with ATIC and H.E.S.S data for cosmic ray electrons: $E^{-10/3}$, E^{-3}, and $E^{-13/3}$

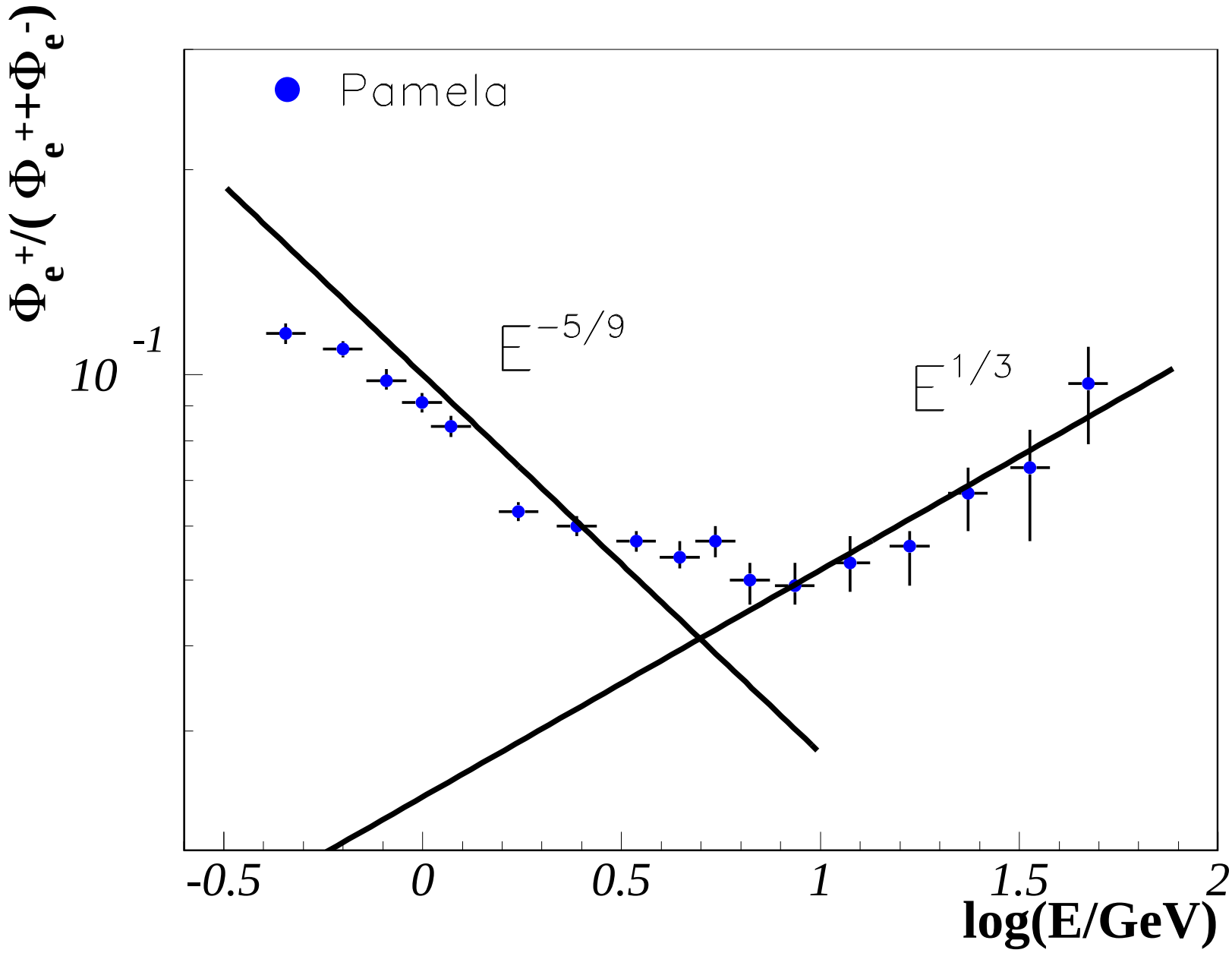

Figure 20 Model prediction with Pamela data for cosmic ray positrons, matching $E^{-5/9}$ at lower energy, and $E^{+1/3}$ at higher energy.

Consequences of massive star physics

- Cosmic ray electrons at low energies sum of $E^{-2.75}$ and $E^{-8/3}$
- Wiggles in spectrum attributable to adiabatic losses, adiabatic compression, and catastrophic losses in magnetic bottles
- The cosmic ray electron spectrum $E^{-10/3}$ at moderate energies, E^{-3} at higher energy,
- and at the highest energies $E^{-13/3}$
- The cosmic ray positron/electron ratio will approach a $E^{-5/9}$ at lower relativistic energy,
- and $E^{+1/3}$ at higher energy

Acknowledgement

Work with PLB was supported by contract AUGER 05 CU 5PD 1/2 via DESY/BMB and by VIHKOS via FZ Karlsruhe; by Erasmus/Sokrates EU-contracts withe the universities in Bucharest, Cluj-Napoca, Budapest, Szeged, Cracow, and Ljubljana; by the Humboldt Foundation; and by research foundations in Korea, China, Australia, India and Brazil.

References

[1] Abbott, D. C., Bieging, J. H., Churchwell, E., The detection of variable, nonthermal radio emission from two O type stars, *Astrophys. J.* **280**, 671 - 678 (1984)

[2] Aharonian, F. A., Atoyan, A. M., & Völk, H. J., High energy electrons and positrons in cosmic rays as an indicator of the existence of a nearby cosmic

[3] V. Barger, W.Y. Keung, D. Marfaitis, G. Shaugnessy, Pamela and dark matter (2008); arXiv:0809.0162

[4] Barvainis, R., McIntosh, G., Predmore, C. R., Evidence for strong magnetic fields in the inner envelopes of late-type stars, *Nature* **329**, 613 - 615 (1987)

[5] Bell, A., The acceleration of cosmic rays in shock fronts. I, *Month. Not. Roy. Astr. Soc.* **182**, 147 - 156 (1978)

[6] Bell, A., The acceleration of cosmic rays in shock fronts. II, *Month. Not. Roy. Astr. Soc.* **182**, 443 - 455 (1978)

[7] Bell, A. R., Lucek, S. G., Cosmic ray acceleration to very high energy through the non-linear amplification by cosmic rays of the seed magnetic field, *Month. Not. Roy. Astr. Soc.* **321**, 433 - 438 (2001)

[8] Bell, A. R., Turbulent amplification of magnetic field and diffusive shock acceleration of cosmic rays, *Month. Not. Roy. Astr. Soc.* **353**, 550 - 558 (2004)

[9] Bell, A. R., The interaction of cosmic rays and magnetized plasma, *Month. Not. Roy. Astr. Soc.* **358**, 181 - 187 (2005)

[10] Bergström, L., Bringmann, T., Edsjö, J., New positron spectral features from supersymmetric dark matter - a way to explain the Pamela data? (2008); arXiv:0808.3725

[11] Biermann, P.L., Cosmic rays I. The cosmic ray spectrum between 10^4 GeV and $3\,10^9$ GeV, *Astron. & Astroph.* **271**, 649 (1993); astro-ph/ 9301008

[12] Biermann, P.L., & Cassinelli, J.P., Cosmic rays II. Evidence for a magnetic rotator Wolf-Rayet star origin, *Astron. & Astroph.* **277**, 691 (1993); astro-ph/9305003

[13] Biermann, P.L., Cosmic rays: origin and acceleration - what can we learn from radio astronomy, invited plenary lecture at 23rd International Conference on Cosmic Rays, 1993, in Proc. "Invited, Rapporteur and Highlight papers"; Eds. D. A. Leahy et al., World Scientific, Singapore, 1994, p. 45

[14] Biermann, P. L., Gaisser, T. K., Stanev, T., Origin of galactic cosmic rays, *Phys. Rev.* **D 51**, 3450 - 3454 (1995)

[15] Biermann, P.L., Supernova blast waves and pre-supernova winds: Their cosmic ray contribution, invited review chapter in "Cosmic winds and the Heliosphere", Eds. J. R. Jokipii et al., Univ. of Arizona press, 1997, p. 887 - 957; astro-ph/9501030

[16] Biermann, P.L., Cosmic ray interactions in the Galaxy, invited lecture at the Nuclear Astrophysics meeting at Hirschegg, in Proc., GSI, Darmstadt, p.

[17] Biermann, P.L., Langer, N., Seo, E.-S.,& Stanev, T., Cosmic Rays IX. Interactions and transport of cosmic rays in the Galaxy, *Astron. & Astroph.* **369**, 269 - 277 (2001)

[18] Biermann, P.L. & Seo, E.-S., Cosmic Radiation, invited review, Academic Press Encyclopedia, Third Edition, vol. 3, p. 823 - 835, 2002

[19] Biermann, P.L., Moiseenko, S., Ter-Antonyan, S., & Vasile, A., Cosmic Rays from PeV to ZeV, Stellar Evolution, Supernova Physics and Gamma Ray Bursts, Invited review at the 9th course of the Chalonge School on Astrofundamental Physics: "The Early Universe and The Cosmic Microwave Background: Theory and Observations"; Eds. N.G. Sanchez & Y.N. Parijski, Kluwer, p. 489 - 516 (2003); astro-ph/0302201

[20] Biermann, P.L., Cosmic rays, stellar evolution and

ing May 2003, Eds. R. Diehl et al., Elsevier, *New Astron. Rev.* **48**, 41-46 (2004); astro-ph/0309810

[21] Biermann, P.L., Galactic cosmic rays, invited review at the spring Aspen meeting 2005, Ed. John Matthews, *IOP Journ. of Phys.: Conf. Ser.*, **47**, 78 - 85 (2006)

[22] Casanova, S., Biermann, P.L., Engel, R., Meli, A., & Ulrich, R., Sources of Cosmic Rays and Galactic Diffuse Gamma Radiation, Cin Proc. INTEGRAL workshop 2004 in Munich, ESA SP-552, München, Germany, p. 521-524, (2004); astro-ph/0403661

[23] Casse, M., Paul, J. A., On the stellar origin of the Ne-22 excess in cosmic rays, *Astrophys. J.* **258**, 860 - 863 (1982)

[24] Churchwell, E., Bieging, J. H., van der Hucht, K. A., Williams, P. M., Spoelstra, T. A. Th., Abbott, D. C., The Wolf-Rayet system WR 147 - A binary

radio source with thermal and nonthermal components, *Astrophys. J.* **393**, 329 - 340 (1992)

[25] Cirelli, M., Strumia, A., Minimal dark matter predictions and the Pamela positron excess (2008); arXiv:0808.3867

[26] Coutu, S., et al., Cosmic ray positrons: are there primary sources?, *Astropart. Phys.* **11**, 429 (1999)

[27] Diehl, R.

[28] Drake, St. A., Abbott, D. C., Bastian, T. S., Bieging, J. H., Churchwell, E., Dulk, G., Linsky, J. L., The discovery of nonthermal radio emission from magnetic Bp-Ap stars, *Astrophys. J.* **322**, 902 - 908 (1987)

[29] Drury, L. O'C., Rep Progr. Phys. 1983

[30] Drury, L. O'C., et al. many papers

[31] Erlykin, A. D., Wolfendale, A. W., A single source of cosmic rays in the range 10^{15} - 10^{16} eV, *Journ. of Physics* **G 23**, 979 - 989 (1997)

[32] Erlykin, A. D., Wolfendale, A. W., Further evidence favouring the single source model for cosmic rays, *Astropart. Phys.* **23**, 1 - 9 (2005)

[33] Erlykin, A. D., Wolfendale, A. W., Cosmic rays and the Monogem supernova remnant, *Astropart. Phys.* **22**, 47 - 63 (2004)

[34] Gayley, K. G., Owocki, St. P., Line-driven Instability Growth Rates in Wolf-Rayet Winds, *Astrophys. J.* **446**, 801 (1995)

[35] Gwinn, *Astrophys. J.* (1989?)

[36] Heger, A., et al., How Massive Single Stars End Their Life, *Astrophys. J.* **591**, 288 - 300 (2003)

[37] H.E.S.S. Collaboration, The energy spectrum of cosmic-ray electrons at TeV energies, *Phys. Rev. Letters* (in press); arXiv:0811.3894

[38] Huh, J.H., Kim, J.E., & Kyae, B., Two dark matter components in N_{DM}MSSM and Pamela data, (2008); arXiv:0809.2601

[39] Hunter, S.D., et al., EGRET Observations of the Diffuse Gamma-Ray Emission from the Galactic Plane, *Astrophys. J.* **481**, 205 (1997)

[40] Kardashev, N.N., Nonstationarity of Spectra of Young Sources of Nonthermal Radio Emission, *Astronomicheskii Zhurnal* **39**, 393 (1962); translated in *Soviet Astronomy* **6**, 317 (1962)

[41] Kingham, R. J., Bell, A. R., Nonlocal Magnetic-Field Generation in Plasmas without Density Gradients, *Phys. Rev. Letters* **88**, id. 045004 (2002)

[42] Kronberg, P.P., Biermann, P.L., Schwab, F.R., The

of a new radio population of supernova candidates, *Astrophys. J.* **291**, 693 (1985)

[43] Lamers, H. J. G. L. M., Cassinelli, J. P., Introduction to stellar winds, Cambridge U Press, (1999)

[44] Langer, N., & Heger, A., Evolution and explosion of Wolf-Rayet stars, in Proc. *Wolf-Rayet Phenomena in Massive Stars and Starburst Galaxies*, 193rd IAU symposium. Eds. K. A. van der Hucht, G. Koenigsberger, & Ph. R. J. Eenens, ASP, p.187 (1999).

[45] Lucek, S. G., Bell, A. R., Non-linear amplification of a magnetic field driven by cosmic ray streaming, *Month. Not. Roy. Astr. Soc.* **314**, 65 - 74 (2000)

[46] Mannheim, K., Schlickeiser, R. (1994)

[47] Meli, A., Biermann, P. L., Cosmic Rays X. The cosmic ray knee and beyond: Diffusive acceleration at oblique shocks, *Astron. & Astroph.* **454**, p. 687 -

[48] Meynet,

[49] Moskalenko, I.V., Strong, A.W., Production and propagation of cosmic ray positrons and electrons, *Astrophys. J.* **493**, 694 (1998)

[50] Niklas, S., Beck, R., A new approach to the radio-far infrared correlation for non-calorimeter galaxies, *Astron. & Astroph.* **320**, 54 - 64 (1997)

[51] Prantzos, N., Doom, C., de Loore, C., Arnould, M., Nucleosynthesis and evolution of massive stars with mass loss and overshooting, *Astrophys. J.* **304**, 695 - 712 (1986)

[52] Prantzos, N., Casse, M., On the production of Al-26 by Wolf-Rayet stars - Galactic yield and gamma-ray line emissivity, *Astrophys. J.* **307**, 324 - 331 (1986)

[53] Prantzos, N., Nucleosynthesis Activity of WR Stars: Implications for 26Al in the Galaxy and Isotopic Anomalies in Cosmic Rays and the Earlier Solar

System, in "Wolf-Rayet Stars and Interrelations with Other Massive Stars in Galaxies": Proc. 143rd Symp. IAU 1990. Eds Karel A. van der Hucht & Bambang Hidayat. IAU Sympos. 143, Kluwer Academic Publishers, Dordrecht, p.550 (1991)

[54] Prantzos, N., Casse, M., Vangioni-Flam, E., Production and evolution of LiBeB isotopes in the galaxy, *Astrophys. J.* **403**, 630 - 643 (1993)

[55] Prantzos, N., Radioactive Al-26 from massive stars - Production and distribution in the Galaxy, *Astrophys. J. Letters* **405**, L55 - L58 (1993)

[56] Prantzos, N., Casse, M., Cosmic rays and gamma rays in early galaxian phases and the cosmic gamma-ray background, *Astrophys. J. Suppl.* **92**, 575 - 578 (1994)

[57] Protheroe, R.J., On the nature of the cosmic ray positron spectrum, *Astrophys. J.* **254**, 391 (1982)

[58] Ptuskin, V., Lukasiak, A., Jones, F.C., Webber, W.R., The modified weighted slab technique: results, ICRC Salt Lake City, vol. 4, p. 291 (1999)

[59] Rickett, *Annual Rev. of Astron. & Astrophys.* (1977)

[60] Rybicki, Lightman, A., 19.. book

[61] Schatz, H., Rare isotopes in the cosmos, *Physics Today*, November, p. 40 (2008)

[62] Seemann, H., & Biermann, P.L., Unstable waves in winds of magnetic massive stars , *Astron. & Astroph.* **327**, 273 (1997); astro-ph/9706117

[63] Sina, R., Biermann, P.L., Seo, E.S., On the description of the turbulent diffusion model, ICRC2001, p. 1916 (2001)

[64] Snowden, et al. (1997)

[65] Tabatabaei, F. S., et al., A multi-scale study of in-

tron. & Astroph. **466**, 509 - 519 (2007a); astro-ph/0701897)

[66] Tabatabaei, F. S., Krause, M., Beck, R., High-resolution radio continuum survey of M 33. I. The radio maps, *Astron. & Astroph.* **472**, 785 - 796 (2007b); arXiv:0706.0261)

[67] Tabatabaei, F. S., et al., High-resolution radio continuum survey of M 33. II. Thermal and nonthermal emission, *Astron. & Astroph.* **475**, 133 - 143 (2007c); arXiv:0708.2484

[68] Völk, H. et al. many papers

[69] Völk, H. J., Forman, M., Cosmic rays and gamma-rays from OB stars, *Astrophys. J.* **253**, 188 - 198 (1982)

[70] Völk, H.-J., Biermann, P. L., Maximum energy of cosmic-ray particles accelerated by supernova remnant shocks in stellar wind cavities, *Astrophys. J.*

[71] Wiebel-Sooth, B., Meyer, H., & Biermann, P.L., Cosmic Rays VII. Individual element spectra: prediction and data, *Astron. & Astroph.* **330**, 389 (1998); astro-ph/9709253

[72] Wiebel-Sooth, B. & Biermann, P.L., Cosmic Rays, invited chapter for Landolt-Börnstein, Handbook of Physics, Springer Publ. Comp., p. 37 - 91, 1999

[73] Yüksel, H., Kistler, M.D., Stanev, T., TeV Gamma Rays from Geminga and the Origin of the GeV positron excess, (2008); arXiv:0810.2784